AGU ADVANCING EARTH AND SPACE SCIENCES

Earth and Space Science

RESEARCH ARTICLE
10.1029/2025EA004281

Global and Regional Ionospheric Response to a Moderate Storm in South America and Antarctica Using a Multi-Instrumental Approach

Y. D. Melendi[1,2,3], M. Bravo[4], M. G. Molina[1,5,6], M. Paz[1], B. Urra[4], L. De Pasquale[7], D. E. Scipión[8], J. Namour[1,5], T. Duran[2,3], and A. Zalizovski[9,10,11]

[1]Tucumán Space Weather Center (TSWC), Facultad de Ciencias Exactas y Tecnología, (FACET-UNT), Tucumán, Argentina, [2]Departamento de Física–Universidad Nacional del Sur, Bahía Blanca, Argentina, [3]Instituto de Física del Sur (CONICET-UNS), Bahía Blanca, Argentina, [4]Centro de Instrumentación Científica, Universidad Adventista de Chile, Chillán, Chile, [5]Consejo Nacional de Investigaciones Científicas y Tecnológicas (CONICET)-UNT, Buenos Aires, Argentina, [6]Istituto Nazionale di Geofísica e Vulcanología (INGV) Roma, Rome, Italia, [7]Facultad Regional Bahía Blanca, Universidad Tecnológica Nacional, Buenos Aires, Argentina, [8]Radio Observatorio de Jicamarca, Instituto Geofísico del Perú, Lima, Perú, [9]Institute of Radio Astronomy, National Academy of Sciences of Ukraine, Kharkiv, Ukraine, [10]National Antarctic Scientific Center of Ukraine, Kyiv, Ukraine, [11]Space Research Centre of Polish Academy of Sciences, Warsaw, Poland

Abstract In this study, we investigate the ionospheric disturbances caused by a moderate geomagnetic storm (maximum Kp = 6) occurring between 26th February and 1 March 2023. Ionospheric response for the coupling between the solar wind, magnetosphere, and ionosphere systems can be observed across various regions of the globe and it may vary according to the local/regional background ionospheric conditions. We analyzed space and ground-based instruments (e.g., ionosondes, total electron content, GUVI imager, incoherent scatter radar) covering from Antarctica to equatorial latitudes in South America. From a global perspective, we observed two ionospheric storms. The first, with a negative phase observed as a significant decrease (>30%) in the F2-layer critical frequency (foF2), occurred on February 27th at 01:00 UT. This negative phase storm was observed in all the considered regions, with the intensity progressively decreasing from higher to lower latitudes. It is worth mentioning that, for the Antarctic station, we consider the local regime of the Weddell Sea Anomaly. The second ionospheric storm occurred during the recovery phase of the geomagnetic storm on 28th February. In this last case, an enhancement above 30% in foF2 was observed only in the low-latitude station. Subsequently, the geomagnetic storm produced a super fountain effect at the Equatorial Ionization Anomaly resulting in the enhancement of foF2.

Plain Language Summary During geomagnetic storms, the ionosphere can experience disturbances due to the interaction between the solar wind and Earth's magnetic field. The critical frequency of the F2-layer (foF2) is a key parameter to analyze the ionospheric disturbances produced by space weather events. Typically, foF2 shows increases or decreases in its values compared to regular days. Using data from various instruments, such as ionosondes, total electron content, and incoherent scatter radar, covering regions from Antarctica to the equator, we examine the ionospheric effects of a moderate geomagnetic storm (Kp = 6) that occurred between 26th February and 1 March 2023. We observed two ionospheric storm phases: A negative phase, on 27th February, resulted in a significant (>30%) decrease in the F2-layer critical frequency (foF2), especially at higher latitudes. A positive phase, on 28th February, during the storm's recovery phase, led to a >30% increase in foF2 at low latitudes, caused by a super fountain effect in the Equatorial Ionization Anomaly. In addition, we analyzed a simultaneous effect in the D-layer in the Antarctic region causing an enhancement in radio wave absorption. This study underscores the global and regional variations in ionospheric responses to geomagnetic storms.

Key Points:

- Global and regional combined ionospheric conditions were studied in response to a moderate geomagnetic storm ranging from Antarctica to Equatorial latitudes and at different ionospheric heights
- Space and ground-based data have been combined to explain and differentiate physical acting mechanisms including those originated from the solar wind-magnetosphere-ionosphere coupling, and local ionospheric features such as the Weddell Sea Anomaly, Equatorial Ionization Anomaly, proving the relevance of multi-instrumental studies
- We focus on South-America showing the relevance of ionospheric measurements in the region

Correspondence to:
Y. D. Melendi,
yamila.melendi@uns.edu.ar

Citation:
Melendi, Y. D., Bravo, M., Molina, M. G., Paz, M., Urra, B., De Pasquale, L., et al. (2025). Global and regional ionospheric response to a moderate storm in South America and Antarctica using a multi-instrumental approach. *Earth and Space Science*, *12*, e2025EA004281. https://doi.org/10.1029/2025EA004281

Received 12 FEB 2025
Accepted 4 JUL 2025

Author Contributions:
Conceptualization: Y. D. Melendi, M. Bravo, M. G. Molina, B. Urra, T. Duran
Data curation: J. Namour
Formal analysis: Y. D. Melendi, M. Bravo, M. Paz, B. Urra
Funding acquisition: M. G. Molina, L. De Pasquale
Investigation: Y. D. Melendi, M. Bravo, M. G. Molina
Methodology: M. G. Molina
Project administration: Y. D. Melendi, M. G. Molina

1. Introduction

Geomagnetic storms involve the exchange of energy due to the interaction of low-energy plasma from the solar wind with the boundary of the magnetosphere. This energy is redistributed within the coupled Magnetosphere-Ionosphere-Thermosphere system through current systems, leading to global disturbances that can be observed

Resources: M. Bravo, M. G. Molina, M. Paz, B. Urra, L. De Pasquale, D. E. Scipión, T. Duran, A. Zalizovski
Supervision: M. G. Molina
Validation: Y. D. Melendi, M. Bravo, M. G. Molina
Visualization: Y. D. Melendi, M. Bravo
Writing – original draft: Y. D. Melendi, M. Bravo, M. G. Molina
Writing – review & editing: L. De Pasquale, T. Duran

in the ionosphere at heights of the F2 layer (Cander & Mihajlovic, 1998; Danilov & Lastovicka, 2001; Gonzalez et al., 1994; Tsagouri et al., 2000).

These ionospheric responses to geomagnetic storms can be observed as disturbances in density distributions, total electron content (TEC), and the current system, and may cause significant space weather impacts (Prölss, 1995; Werner et al., 1999; Zolesi & Cander, 2014). These disturbances in the ionosphere can manifest as enhancements or depletions in the electron density in the F2 layer relative to a background level (Fang et al., 2012). They are known as ionospheric storms, with positive and negative phases respectively, and occur at altitudes ranging from 200 to 1,000 km (Buonsanto, 1999; Danilov, 2013; Molina et al., 2020).

Different physical mechanisms contribute to the formation of ionospheric storms, such as global thermospheric circulation driven by changes in O/N_2 ratio (Balan et al., 2010; Mikhailov et al., 1995; Mikhailov & Perrone, 2009; Prölss, 1995), as well as changes in temperature, electric fields, and plasmaspheric flux, among others (Prölss, 1995; Rishbeth, 1991).

High latitudes are directly influenced by the interaction between the interplanetary magnetic field (IMF) and the geomagnetic field. This direct coupling, through the geomagnetic field open lines, facilitates the transfer of significant energy from the magnetosphere to the ionosphere during geomagnetic storms. These disturbances, particularly in the high-latitude regions, induce thermospheric circulation changes and plasma convection driven by two main processes: the Prompt Penetration Electric Field (PPEF) and the Joule heating effect. The PPEF accelerates plasma and enhances its redistribution, causing rapid ionospheric disturbances, while Joule heating in the lower thermosphere generates localized thermal expansion and alters the thermospheric composition by depleting the O/N_2 ratio. This depletion reduces the availability of atomic oxygen necessary for ion production, which, combined with the downward transport of air through atmospheric circulation, leads to a decrease in electron density at lower latitudes in the F2 region. These combined effects result in a negative ionospheric storm, originating at high latitudes due to direct coupling with the interplanetary electric field and extending to lower latitudes through thermospheric circulation and plasma redistribution (Danilov, 2001; Richmond, 2021).

While high-latitude ionospheric regions are directly affected by interplanetary magnetic activity, the equatorial and low-latitude regions are not coupled in the same way. However, during geomagnetic storms, these regions can be disturbed through electrodynamic coupling with high latitudes, by PPEF, and through disturbance dynamo electric fields (DDEF). The DDEF, which results from changes in thermospheric circulation due to auroral heating, acts over a time scale of hours to days after the Sudden Storm Commencement (SSC). These fields lead to the redistribution of plasma, causing increases in electron density at low and equatorial latitudes, which may trigger positive ionospheric storms (Ambili & Choudhary, 2023; Kane, 2005; Scherliess & Fejer, 1997).

The behavior of the ionosphere during geomagnetic perturbed days includes an enhancement/suppression of the well-known Equatorial Ionization Anomaly (EIA; Appleton, 1946). The equatorial ionosphere zone is characterized by the $\mathbf{E} \times \mathbf{B}$ upward drift (called electrodynamic drift) of the ionization and tends to generate the "fountain effect", a poleward displacement from the anomaly crest by the diffusion down the magnetic field lines. But during the main phase of geomagnetic storms, a positive PPEF during daylight hours generates an eastward component, and this increase in the upward drift generates an expansion of the diffusion towards higher latitudes, causing a "super fountain effect" (Balan et al., 2010; Rishbeth et al., 2010; Tanaka & Ohtaka, 1996; Wang et al., 2021).

In this complex scenario, where global forcing interacts with regional ionospheric conditions, this work aims to contribute to a better understanding of the ionospheric effects triggered by the geomagnetic storm of the 26 February 2023.

This geomagnetic storm has been reported in several studies. Tariq et al. (2024) analyzed the storm's impact using TEC data from stations in the low-to-mid latitude transition region of the American and Asian sectors. They observed significant variations during the recovery phase, primarily attributed to PPEF, DDEF, and O/N_2 depletion. Reznychenko et al. (2024) focused on comparing ionosonde parameters (the peak height, hmF2, and the maximum electron density, NmF2) with the IRI model. The work of Sun et al. (2023) highlighted the extension of plasma bubbles to mid-latitudes over East/Southeast Asia, which they attributed to rapid upward vertical plasma drifts over the magnetic equator, possibly driven by PPEFs. Similarly, Bojilova and Mukhtarov (2023) studied the impact of the same ionospheric storm, focusing on sudden stratospheric warming and its effects over Europe through a latitudinal analysis. Aa et al. (2023) analyze the ionospheric response at the European and North

American longitude sectors. Finally, Starodubtsev et al. (2024) studied magnetohydrodynamic waves in solar wind plasma during this storm.

In this work we investigate the ionospheric disturbances in South America and Antarctica observed during the moderate geomagnetic storm (maximum Kp = 6) between 26th February and 1 March 2023. The study region encompasses a range of geomagnetic latitudes, including equatorial regions influenced by the EIA, low latitudes affected by the EIA crests, and mid-latitudes that include the Weddell Sea Ionospheric Anomaly (WSA). The WSA, located over the Antarctic Peninsula, represents a distinctive ionospheric feature characterized by an anomalous enhancement of electron density. First reported in 1958 (Bellchambers & Piggott, 1958), the WSA is notable for exhibiting a pronounced diurnal maximum during the local summer near midnight, which contrasts with the more typical ionospheric behavior that peaks around local noon. This unusual temporal pattern has been linked to complex interactions between neutral winds, magnetic field geometry, and ionospheric dynamics specific to the Antarctic region (Bravo et al., 2025; Chang et al., 2015; Karpachev et al., 2011; Zalizovski et al., 2021). We use space and ground-based instruments to explain the global ionospheric response as well as local/regional observed conditions using a multi-instrumental approach.

The paper is organized as follows, the Data and Methodologies section describes in detail the data, data treatment, instruments, and the main methodology used. In the subsequent section, Global parameters, the solar wind conditions and geomagnetic indices are described to characterize the geomagnetic storm. In the Global and Regional Ionospheric Impacts section, the results of the analysis are presented, detailing the changes observed at each considered ionospheric station in South America and Antarctica. Finally, the discussions and conclusions of this study are presented.

2. Data and Methodologies

We analyzed different solar wind parameters, such as the total interplanetary magnetic field (Bt) and its z-component (Bz), proton density (N), plasma velocity (V), and temperature (T) (provided by SWPC-NOAA, https://www.ngdc.noaa.gov/) to understand the solar wind-magnetosphere coupling and the onset of the geomagnetic storm. To characterize the global geomagnetic conditions, the geomagnetic indices Kp (https://kp.gfz-potsdam.de/)and Sym-H (https://wdc.kugi.kyoto-u.ac.jp/) were considered. Since the study region corresponds to the South American sector, we also find it appropriate to use the South American geomagnetic index Ksa, which is derived from measurements from the EMBRACE magnetometer network (Denardini et al., 2015, https://www2.inpe.br/climaespacial/portal/en/).

To analyze the global and regional ionospheric response in South America and Antarctica region, we considered the F2-layer critical frequency (foF2) from ionosondes obtained by ionospheric stations located from Equatorial to middle geomagnetic latitudes, and the vertical Total Electron Content (vTEC) derived from Global Navigation Satellite System (GNSS). Ionosondes are high-frequency (HF) radars capable of measuring the virtual height of the ionosphere as a function of frequency through vertical soundings. The resulting data is presented graphically in the form of ionograms. The foF2 represents the frequency at the height in which maximum ionospheric reflectivity occurs and in general, it is in agreement with the maximum electron density.

We considered four ionosondes distributed latitudinally in South America-Antarctica, covering from equatorial to mid-geomagnetic latitudes. These HF radars were of three different types and thus, we considered their particular settings to process and compare the data.

As part of the data processing, we used manually validated foF2 obtained from a vertical incidence pulsed ionospheric radar system at an equatorial station in Jicamarca, Perú (12°S; 76.8°W) with a temporal resolution of 5 min.

Two Advanced Ionospheric Sounders developed by the Istituto Nazionale di Geofisica e Vulcanologia (AIS-INGV) ionosonde systems with a temporal resolution of 10 min were also considered. The ionosondes are located in a mid-latitude ionospheric station in Bahía Blanca (38.7°S; 62.3°W) and a low latitude ionospheric station in Tucumán (26.9°S; 65.4°W), both deployed in Argentina and managed by the Tucumán Space Weather Center (TSWC) in FACET-UNT. For operative purposes, data is automatically scaled using "Autoscala" software (Scotto & Pezzopane, 2000) after each sounding to estimate key ionospheric parameters, including the critical frequencies of various ionospheric layers (foF2, foF1, and fEs), as well as parameters such as the MUF(3,000)F2

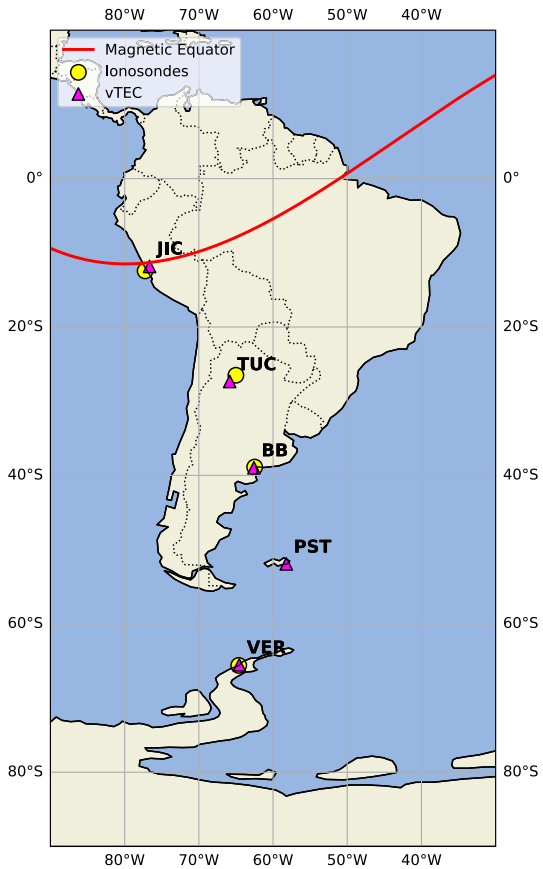

Figure 1. Map showing the locations of ionospheric stations.

(Bianchi et al., 2013; Cabrera et al., 2010; Molina et al., 2016). In addition, the data used in this work was manually corrected to avoid possible errors from the automatic scaling process.

The southernmost ionosonde used corresponds to the Akademik Vernadsky ionospheric station (65.2°S; 64.3°W) in Antarctic Galindez Island, Argentine Islands Archipelago. It is an IPS-42 ionosonde sharing an antenna with a digital ionosonde based on software-defined radio (SRD) technology. We used data manually scaled from the SRD ionosonde plus a redundant control with the other ionosonde, with a temporal resolution of 1 hr (Koloskov et al., 2023). Figure 1 and Table 1 show the details of each of the mentioned ionospheric stations including vTEC and ionosonde data.

Regarding vTEC, it was derived from GNSS receivers data by calibrating the Receiver Independent Exchange (RINEX) format using GPS-TEC software version 2.9.5 developed by Gopi Seemala (Seemala & Valladares, 2011, http://seemala.blogspot.com). This software determines the slat TEC (sTEC) from pseudo-range measurements from RINEX files only for GPS constellations. Next, satellite elevation and azimuth angles are used in the calculation of vTEC from sTEC.

We obtained TEC distributions over South America using the RINEX files from the International GNSS Service network (IGS, www.igs.org; Dow et al., 2009), from the Low-Latitude Ionospheric Sensor Network (LISN, http://lisn.igp.gob.pe), from the Rede Brasileira de Monitoramento Contínuo de Sistemas GNSS (RBMC, www.ibge.gov.br), from the Red Argentina de Monitoreo Satelital Continuo (RAMSAC, www.ign.gob.ar; Piñón et al., 2018) and from Centro Sismológico Nacional network (CSN, www.sismologia.cl). TEC for each station is calculated from median vTEC values from measurements with ionospheric piercing points localized to within ±2° latitude and longitude during a ±5 min interval.

In order to add information between the continent and Antarctic regions, we included TEC from the Port Stanley station (51.6°S; 57.9°W). Unfortunately, the ionosonde in Port Stanley discontinued its measurements in 2019.

To identify ionospheric perturbations at heights of the F layer in ionosonde data, we compare the current value of foF2 with a background level. To obtain the background level we used the deviation between the observed foF2 and the median of the 27 previous days (Equation 1).

$$\delta\text{foF2} = \frac{\text{f0F2(obs)} - \text{f0F2(med)}}{\text{f0F2(med)}} \quad (1)$$

where foF2(obs) corresponds to the observed value of foF2, and foF2(med) corresponds to the median of foF2 values of 27 days (Danilov, 2001). For the 27-day median, we used the date range from January 26th to 21 February 2023.

Table 1
Ionospheric Stations With Their Geographic and Geomagnetic Coordinates (Source: https://wdc.kugi.kyoto-u.ac.jp/igrf/gggm)

Station	Geographic coordinates	Geomagnetic coordinates
Jicamarca (JIC)	12°S; 76.8°W	2.7°S; 4°W
Tucumán (TUC)	26.9°S; 65.4°W	17.5°S; 6.8°E
Bahía Blanca (BB)	38.7°S; 62.3°W	29.4°S; 9.3°E
Port Stanley (PST)	51.6°S; 57.9°W	42.7°S; 12.5°E
Vernadsky (VER)	65.2°S; 64.3°W	55.9°S; 6.3°E

To understand the physical changes in the ionosphere due to the storm, other parameters were analyzed, such as changes in thermospheric composition, and vertical drifts in the equatorial region.

The spatial scanning ultraviolet spectrograph GUVI (Global UltraViolet Imager, https://guvitimed.jhuapl.edu/) measures the composition and temperature profiles of the MTI region, as well as its auroral energy inputs. We used the O/N_2 ratio product derived from the GUVI instrument to analyze changes in the thermosphere composition.

To understand the complex equatorial ionospheric response to the geomagnetic storm, we added data from the Jicamarca Incoherent Scatter Radar

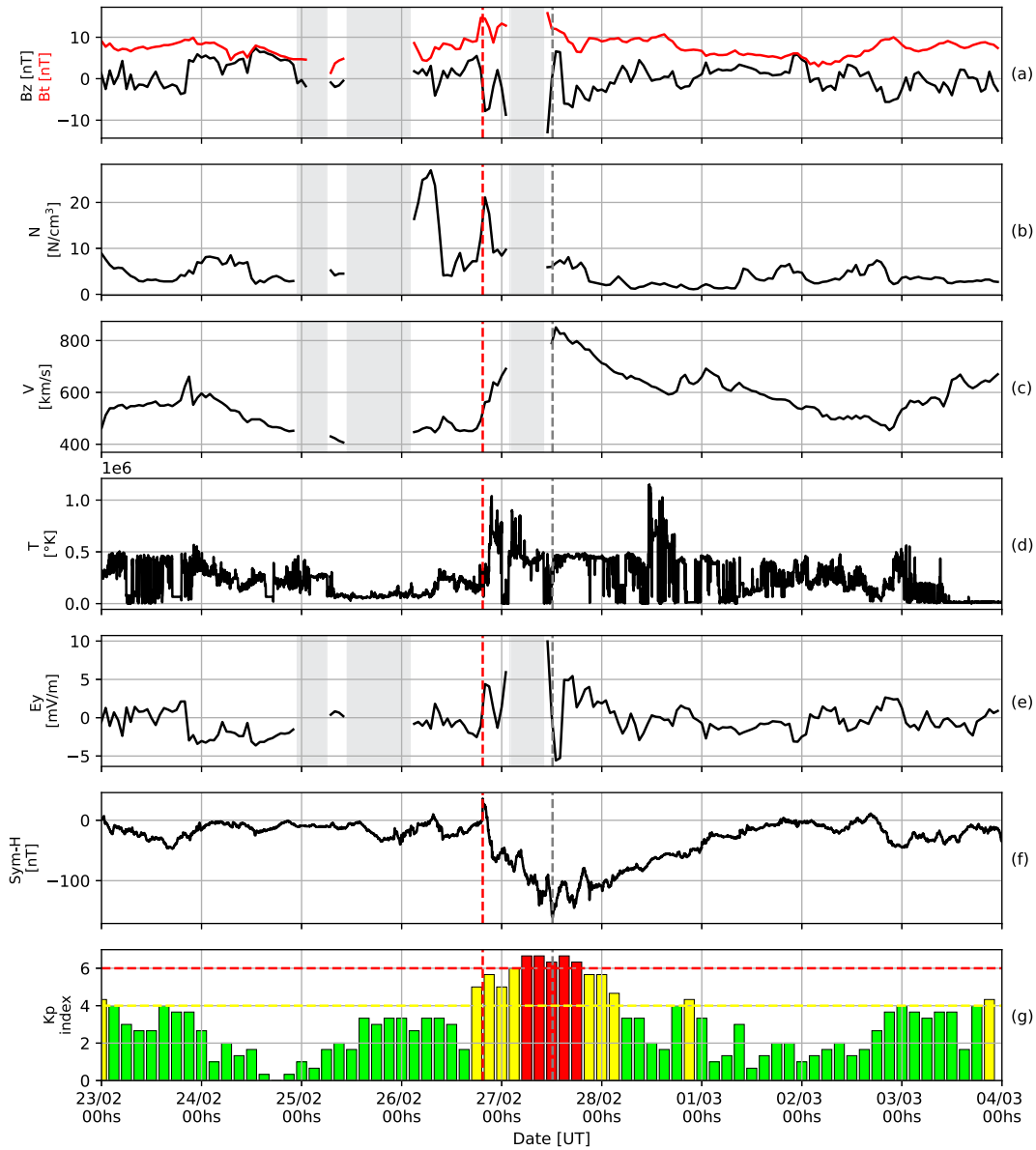

Figure 2. Panels showing (from top to bottom): (a) Total IMF and z-component of IMF(Bt, Bz) in red and black line, respectively, (b) Proton density (N), (c) Plasma speed (V), (d) Temperature (T), (e) y-component of the electric field (Ey), (f) Sym-H index, and (g) Kp index. Vertical red line indicates Sudden Storm Commencement, the gray line represents the main phase pick, and the shaded areas correspond to data gaps.

(ISR). This radar measures plasma density, temperature, composition, and drift in the equatorial zone. In particular, in this study, we used the Jicamarca Unattended Long-term Investigations of the Ionosphere and Atmosphere (JULIA) experiment for evidence of vertical drifts.

3. Global Parameters

The global development of the geomagnetic storm was described using solar wind data and geomagnetic indices. Figure 2 displays solar wind parameters such as the interplanetary magnetic field (IMF), in particular, the total IMF (Bt) and IMF z-component (Bz), the proton density (N), plasma velocity (V), temperature (T), and y-component electric field (Ey), in comparison with the geomagnetic index Sym-H.

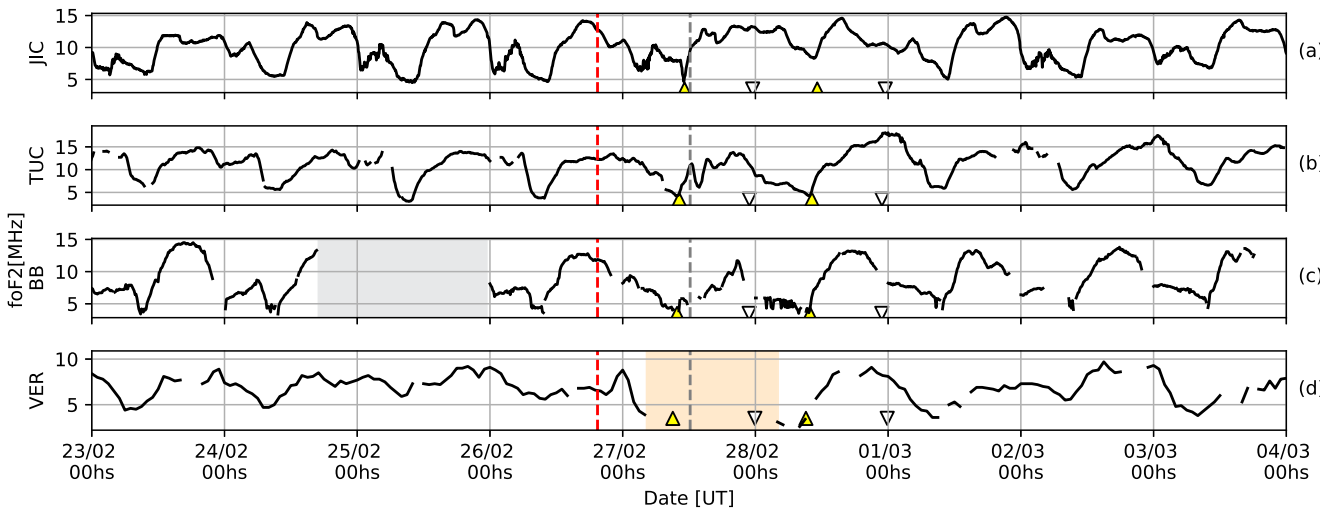

Figure 3. F2-layer critical frequencies from each ionosonde station ((a)Jicamarca, (b)Tucumán, (c) Bahía Blanca, and (d)Vernadsky) are shown from 23rd February to 4th March 2023. The red dashed line represents the Sudden Storm Commencement, while the gray dashed line indicates the peak of the main phase. The shaded areas correspond to data gaps: the gray area corresponds to technical issues, while the orange area corresponds to absorption. The yellow triangles indicate the local sunrise time, while the white inverted triangles represent the local sunset time.

The solar wind magnetic field configuration when Bz becomes negative may be favorable for the development of magnetic reconnection between the solar wind's magnetic field lines and the magnetosphere (Tsurutaniet al., 2020). As observed in Figure 2a, Bz turns negative on 26th February and Bt has a marked increase.

Simultaneously, N, V, T, and Ey increase their values showing a structure in the solar wind reaching the geospace. N reached ∼21 N/cm^3 immediately as Bz began negative but had a sudden decrease 2 hr later (see Figure 2b). V and T exhibit abrupt increases and then show a decrease for a couple of hours (Figures 2c and 2d, respectively). At this point, a gap occurs in the data for all parameters (except for temperature) which continues until 27 mid-February. Following this gap, some components drop rapidly, while others gradually return to quiet conditions. The plasma velocity reached 851 km/s (not considering the gap).

In the Sym-H index (see Figure 2f), the SSC is observed as a maximum value of 36 nT on 26th February at 19:27 UT showing the onset of the geomagnetic storm (vertical dashed line). Following the SSC, Sym-H sharply decreased, initiating the main phase of the geomagnetic storm. This main phase reached a minimum value of −161 nT on 27th February at 12:12 UT with a duration of approximately 16 hr. From this point on, the Sym-H index began to gradually recover. The duration of the recovery phase is approximately 2 days and 6 hr. The geomagnetic storm had a total duration of approximately 3 days.

In concordance with the Sym-H index, the Kp index reached a maximum of 6 on 27th February and remained at these values between 06:00 and 21:00 UT (see Figure 2g). According to NOAA geomagnetic scales, this value is cataloged as a G2 storm or moderate storm. Ksa shows a similar behavior for South America (not shown here).

4. Global and Regional Ionospheric Impacts

In this section, we present the response in the ionosphere for South America, from Antarctic to Equatorial regions, and we also discuss the main regional conditions acting in combination with the geomagnetic storm. In particular, we show how the complex equatorial electrodynamics produces a regional impact at a low-latitude station when the extra energy input from the geomagnetic storm is also present. Moreover, we show how the local WSA regime can affect the analysis at the Antarctic station. Finally, we include the analysis of space weather impact on the lower ionosphere (D-layer) in the Antarctic station.

Figure 3 shows the foF2 parameter for each of the mentioned stations in Figure 1, the vertical red dotted line indicates the SSC and the vertical gray dotted line indicates the minimum Sym-H (main phase pick). The gray-shaded area at the Bahía Blanca station corresponds to technical issues, while the orange-shaded area at the Vernadsky station is attributed to absorption. The yellow triangles indicate sunrise, while the white ones represent

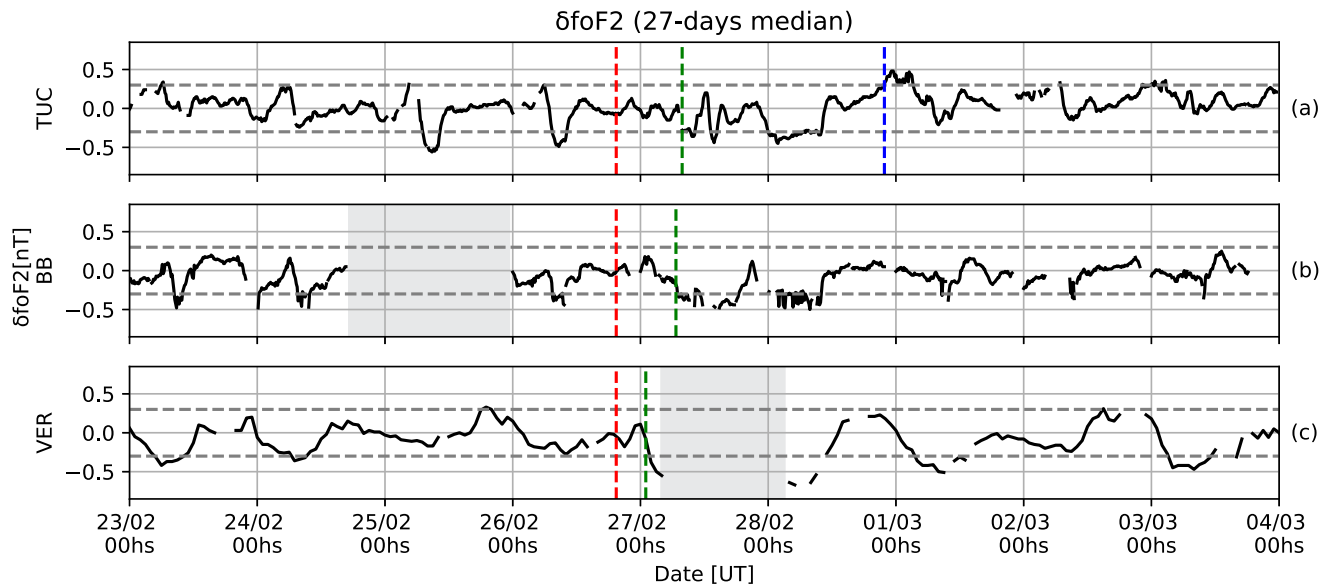

Figure 4. Deviation from the 27-day median of the F2-layer critical frequency for three ionosonde stations ((a) Tucumán, (b) Bahía Blanca and (c) Vernadsky) from 23rd February to 4th March 2023. The red line indicates the Sudden Storm Commencement, the green line represents the negative phase onset, and the blue line indicates the positive phase onset. The horizontal dotted gray lines mark the 30% deviation.

sunset. At first glance (Figure 3), it can be observed that after the main phase, the four stations show atypical behavior in comparison with the other days.

The reason for the gap is polar absorption in Vernadsky as one of the ionospheric responses to the geomagnetic storm. This is also a local space weather effect in polar regions that will be further discussed in the discussion section.

In Tucumán and Bahía Blanca, during the night after SSC, the foF2 values seem to have decreased in comparison with the previous days (see Figures 3b and 3c, respectively). This situation occurs in concordance with the main phase of the geomagnetic storm. Similar behavior can be observed at Vernadsky station (Figure 3d) until the measurements stopped before the end of the geomagnetic storm main phase. The gray dashed line shows the end of the geomagnetic storm main phase (minimum Sym-H value). These initial observations suggest the presence of a global perturbation or response triggered by the geomagnetic storm.

Additionally, the values in Tucumán show an increase compared to the values of the previous days during the nighttime hours of 28th February. This suggests ionospheric perturbations occurring in the equatorial region due to local conditions and the recovery phase of the geomagnetic storm. While in Jicamarca, on 28th February it can be observed high values of foF2 (Figure 3a). It is especially interesting to observe that the minimum foF2 on the 28th February night is significantly higher than the other days.

We further analyzed these initial observations by defining increases or decreases relative to the averaged values (δfoF2) for each station, as previously mentioned in Equation 1.

Due to the lack of data availability at Jicamarca, this deviation is only calculated for Tucumán, Bahía Blanca, and Vernadsky stations (see Figure 4). Many authors suggest a threshold of 15% deviation to consider a value anomalous (e.g., Fang et al., 2012; Ippolito et al., 2020; Kutiev & Muhtarov, 2001). Nevertheless, and with the aim of carrying out a more strict analysis, we established a 30% threshold value to identify periods of intense disturbances, represented in Figure 4 as dotted horizontal lines. Data points that exceed this threshold are identified as a positive ionospheric storm phase, while those below the negative threshold represent a negative ionospheric storm phase (Balan et al., 2010; Molina et al., 2020; Prölss, 1995; Reznychenko et al., 2024).

On 27 February, a negative phase was observed at all stations, starting at 1:00 UT in Vernadsky, at 6:40 UT in Bahía Blanca, and at 7:50 UT in Tucumán. The local time in this region is the same, with LT = UT- 4. In brief, the negative phase occurred approximately 5 hr and 30 min later in Bahía Blanca and 6 hr and 30 min later in

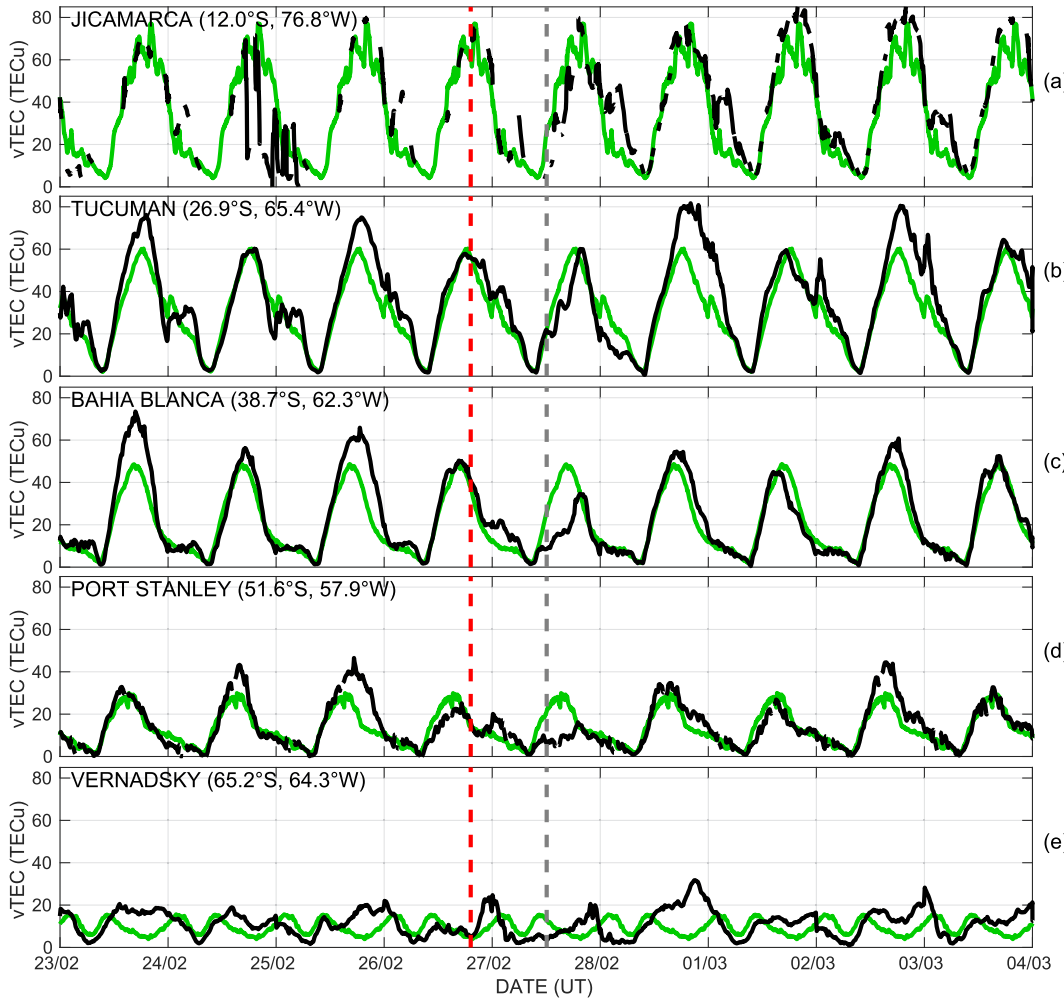

Figure 5. Vertical total electron content for five ionospheric stations ((a) Jicamarca, (b) Tucumán, (c) Bahía Blanca, (d) Port Stanley, and (e) Vernadsky) from 23rd February to 4th March 2023. The red dotted vertical line indicates the sudden storm commencement, the gray line represents the main phase pick, the black line corresponds to observations, and the green line represents monthly median values for each station.

Tucumán after the onset of the negative phase in Vernadsky, suggesting that the disturbances were transported from the pole to lower latitudes.

Additionally, between 28th February at 19:20 UT and 1st March at 03:30 UT (LT = UT−4), a positive ionospheric storm phase is observed only at Tucumán station. This situation is not observed in Bahía Blanca and Vernadsky, suggesting another source of the perturbations.

It is important to note that, comparing Vernadsky in Figures 3d and 4c, both curves (foF2 and δfoF2) show similar behavior. This similarity is due to the fact that the 27-day quiet median has almost constant values between 7 and 8.5 MHz. This is because, typically, February is a transitioning month between the WSA and the normal foF2 regime (see Bravo et al., 2025). A thorough day-by-day analysis shows that the first half of the month has a maximum of foF2 during the night, while the second half has a maximum at midday.

We confirmed the presence of negative and positive phases of an ionospheric storm using the vTEC. Figure 5 shows vTEC between 23 February to 04 March 2023 the previously mentioned ionospheric stations: Jicamarca (equatorial station), Tucumán (low-latitude station), Bahía Blanca, and Port Stanley (mid-latitude stations), and Vernadsky (Antarctic station).

Observing the panels shown in Figure 5, a decrease in vTEC is observed globally across all stations a few hours after SSC in concordance with the observed behavior of foF2, with a more significant decrease in the negative phase at Vernadsky and Port Stanley stations compared to those located at lower latitudes.

However, it can be observed that the quiet Vernadsky curve does not represent the variability either before or after the geomagnetic storm. This is due to the reasons mentioned above for the foF2 at Vernadsky, namely that February is the transition month between the WSA and the normal regime.

In the case of Jicamarca, the limited number of available GNSS receivers means that the analyzed days have many gaps, even when considering the region within ±2° latitude and longitude during a ±5-min interval.

The positive phase can also be identified only at Tucumán station, reinforcing the regional ionospheric response at equatorial and low latitudes. On the other hand, in the case of TEC, a significant enhancement is also observed at the Vernadsky station during the last hours of 28th February.

5. Discussions

When analyzing the ionospheric response to geomagnetic storms, both the global perturbations and the local or regional conditions should be considered. For example, common reference methodologies involve using the 27-day median prior to the storm or selecting the 5–10 geomagnetically quietest days of the month. However, these approaches may not be optimal for stations affected by local phenomena. Particularly, in locations influenced by the WSA, such as Vernadsky, the typical reference patterns may fail to capture the actual background behavior. During December and January, Vernadsky consistently exhibits an abnormal diurnal variation, with peak values occurring around local midnight rather than the usual daytime maximum. Mid-February marks a transitional period in which the maximum gradually shifts toward local noon, and by March, the diurnal variation returns to a normal pattern. The timing of this transition is diffuse and modulated by the level of solar activity (Bravo et al., 2025; Zalizovski et al., 2021). As a result, using standard reference days during these months can lead to a misinterpretation of storm-time effects, potentially underestimating or overestimating positive and negative ionospheric responses, as observed in both foF2 and TEC measurements.

Observing Figures 3–5, after the SSC, we can identify two phases (negative and positive) separated by a time range of more than a day. The first phase occurs during the main phase of the geomagnetic storm and can be observed globally in all the analyzed stations, while the second phase develops during the recovery phase and is observed only in the equatorial region. To understand the mechanisms that act and generate ionospheric disturbances, we will discuss the negative and positive phases separately.

In the negative phase case, we compared GUVI images between 26th February and 1 March 2023 (see Figure 6) and in these images, a low oxygen-nitrogen ratio can be observed, moving from high latitudes in the southern hemisphere to lower latitudes on 27th February, lasting one day. Starting the next day, the values of the oxygen-nitrogen ratio return to their previous levels.

Comparing the GUVI images (see Figure 6) with the deviation from the median of 27 days (see Figure 4), we notice simultaneously the decrease of foF2 with changes in the variations of the O/N_2 ratio.

Additionally, when observing foF2, there is a time difference of 5 hr and 40 min between Bahía Blanca and Vernadsky, and 6 hr and 50 min between Tucumán and Vernadsky, which indicates a delayed response from higher latitudes to lower latitudes. The decrease in foF2 occurs earlier at Vernadsky than at Bahía Blanca and Tucumán, reinforcing the phenomenon observed in the GUVI images. For these reasons, we suggest an ionospheric perturbation initiated in high latitudes and traveling to mid and low latitudes due to thermospheric expansion as a result of Joule heating. We suggest that this mechanism is acting in combination with PPEF which can be observed when Bz turns negative in the solar wind (Figure 2) during the main phase of the geomagnetic storm. Changes in thermospheric composition and PPEF are acting as the main physical mechanisms responsible for the negative phase (Sun et al., 2023; Tariq et al., 2024).

The Mid-latitude Ionospheric Trough is a nighttime depletion of plasma density located in the subauroral F region of the ionosphere. It typically spans roughly 10 degrees of latitude and is detectable at all longitudes. The trough structurally consists of three distinct components: a polar boundary, a trough minimum, and an equatorward boundary. This structure predominantly appears during nighttime hours and shows notable changes under geomagnetically disturbed conditions. During geomagnetic storms, the trough often shifts toward lower latitudes

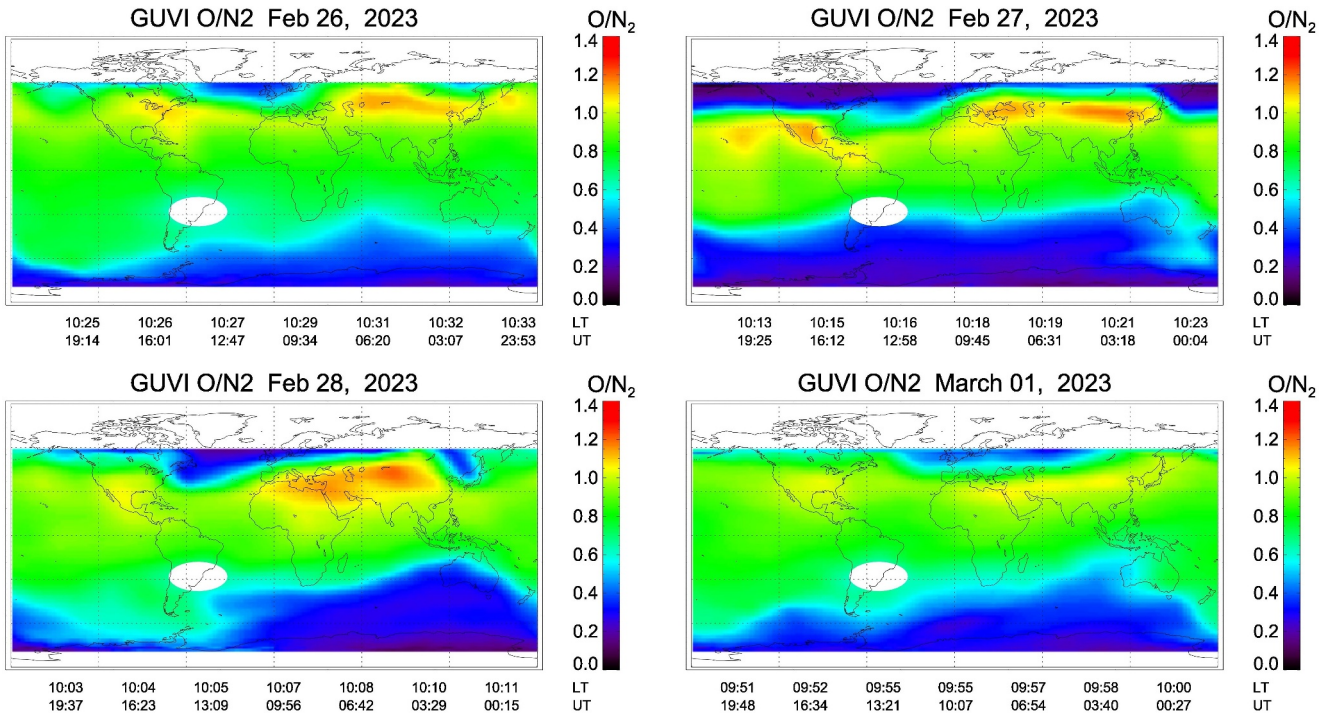

Figure 6. The images from Global UltraViolet Imager (GUVI) instrument show thermospheric O/N_2 ratio on disk measured in the L3 layer between 26 February and 1 March 2023.

as a result of the equatorward expansion of the auroral oval and enhanced high-latitude convection. This displacement often leads to significant negative ionospheric storm effects, characterized by a marked decrease in electron density compared to quiet-time levels at mid-latitudes. While previous research has linked the equatorward movement of the trough with these negative storm effects, it remains unclear whether the displacement consistently results in such ionospheric depletions or if all negative ionospheric storm effects near the trough are directly associated with its equatorward shift (Huang et al., 2018; Mošna et al., 2024; Nayak et al., 2016; Yang et al., 2022).

It is important to note that the equatorward movement of the trough during geomagnetic storms is not always accompanied by a negative ionospheric storm effect, nor is the negative ionospheric response around the trough position necessarily associated with its displacement (Yang et al., 2022). In fact, if we look at the low values observed at Vernadsky station in Figure 5, we can see that no significant changes are observed during the event.

Regarding the positive phase, since the perturbations are present only in the low-latitude station (Tucumán), we must consider a different physical mechanism. Since the increase in foF2 observed in the equatorial and sub-equatorial regions occurs during the recovery phase, nearly two days after the SSC, we infer that it is associated with changes in thermospheric circulation due to auroral heating, which take this amount of time to reach these latitudes, evidencing the presence of DDEF. Although Vernadsky appears to show an enhancement in Figure 5, this can be misleading. It is important to remember that vTEC represents the total electron content integrated over the ionospheric column, and high vTEC values do not necessarily imply high f0F2 values. In fact, when checking Figure 4, no increase in f0F2 beyond the threshold is observed at Vernadsky during that time. This is consistent with what is shown in Figure 4, where Vernadsky clearly remains below the defined threshold.

During the daytime, additional electric fields into the equatorial ionosphere will uplift the plasma and transport it to poleward latitudes. Due to solar photoionization, the plasma densities will be restored to typical values (higher TEC values) that, in combination with the plasma transport, will produce an enhancement of the EIA called the "dayside ionospheric super-fountain (DIS) effect." This enhancement will create a positive ionospheric storm (Tsurutani et al., 2008).

10.1029/2025EA004281

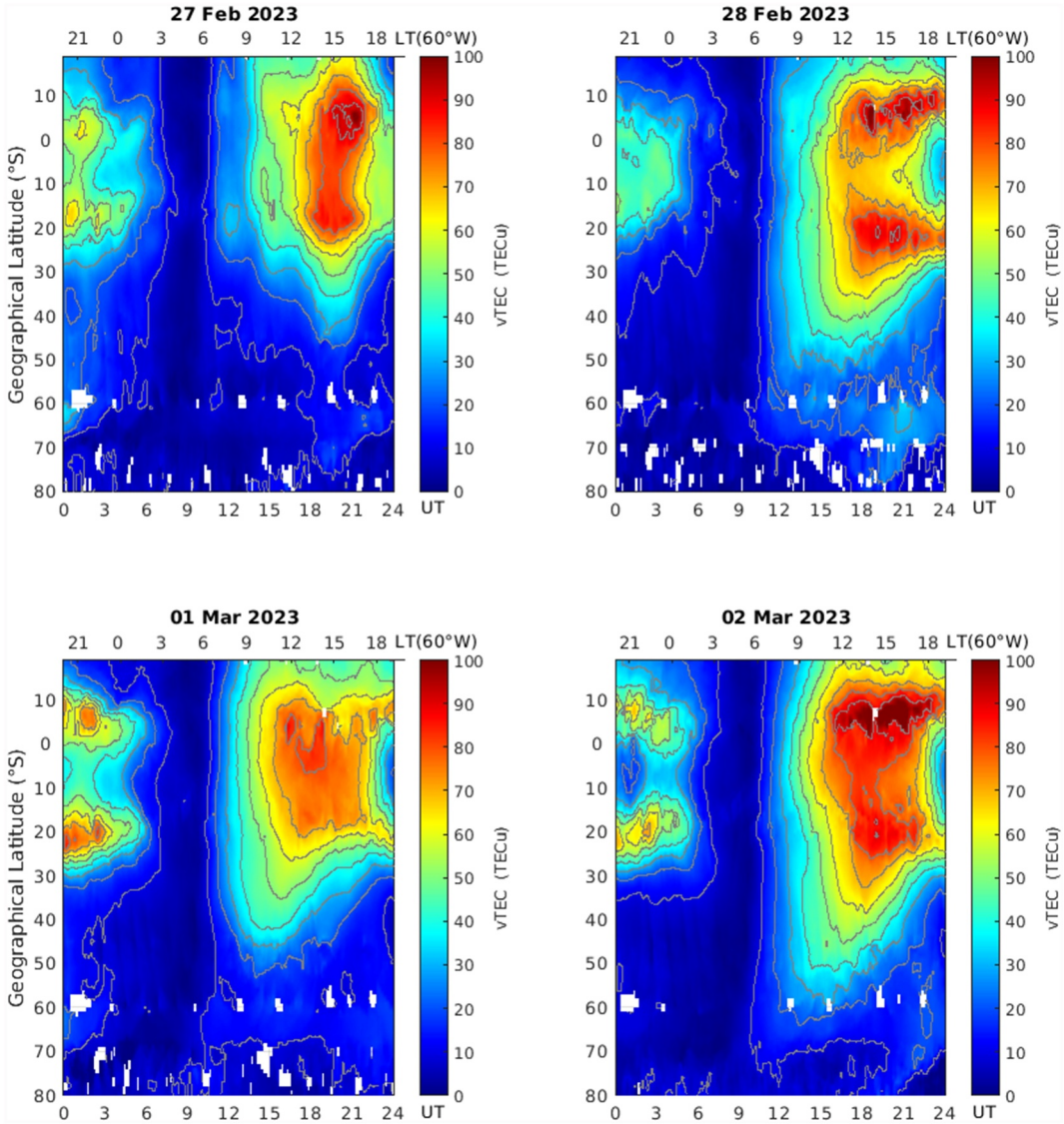

Figure 7. Diurnal variation of total electron content along the geographic meridian of Bahía Blanca Station during 27 February, 28 February, 1 March, and 2 March 2023.

To reinforce this hypothesis, we analyzed the data of TEC for the South American region along the geographic meridian of Bahía Blanca station on the day before and after the onset of the positive phase (see Figure 7). Figure 7 shows four consecutive days of TEC maps from equatorial latitudes (20°N geographic latitude) to the Antarctic region (80°S geographic latitude) for a fixed longitudinal of 62.3°W. By comparing the four days, it can be observed that during the 28th at daytime (see around 9:00 to 20:00 LT), there is an enhancement of TEC and expansion to higher latitudes of EIA crests which is consistent with a DIS effect. For example, on the 28th the well-defined crests show TEC values on the scale of 80–100 TECu at both sides of the equator. Moreover, these high TEC values (>90 TECu) can be observed at different locations within the crests. When compared with the previous and the next day, these enhancements are very significant. Another feature to observe is that higher TEC values, during the DIS effect, last until later hours in comparison with the 27th February and 01st March. On the other hand, we observed a decrease in vTEC values at the equatorial station during this period compared to the previous days (see Figure 7).

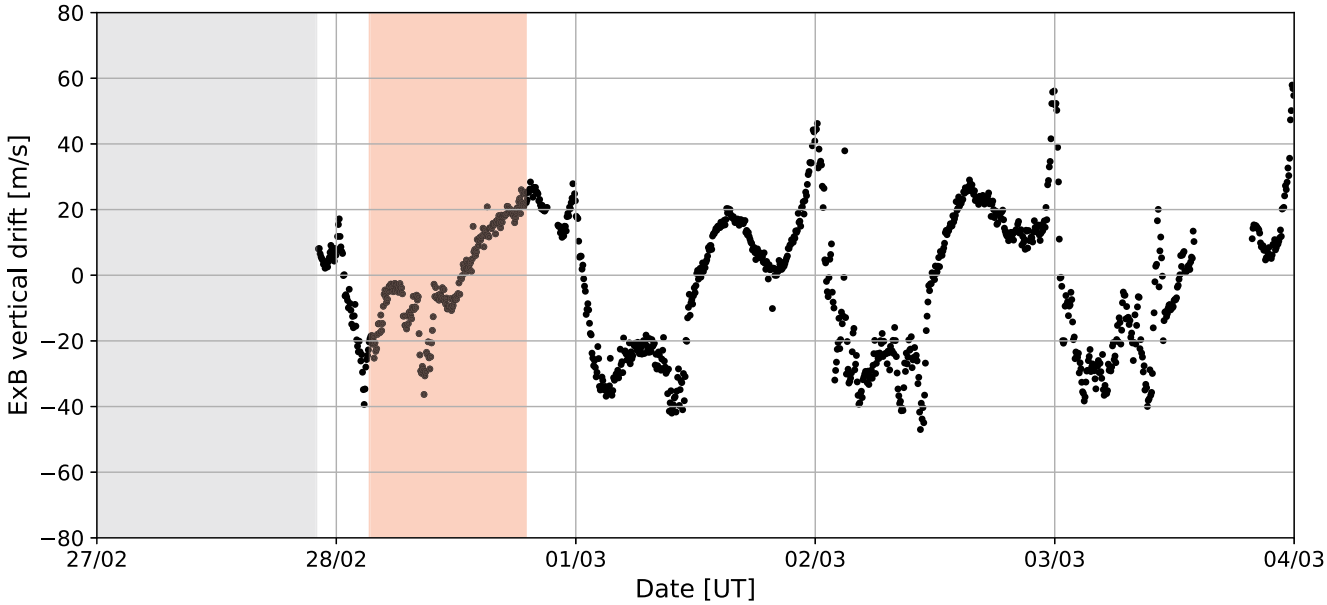

Figure 8. Vertical drift at Jicamarca station from 27th February to 4 March 2023 (LT = UT-5). The gray shaded area corresponds to data gap, while the red shaded area corresponds to enhancement values with respect to consecutive days.

To confirm the DIS effect, Figure 8 shows the vertical drift (ExB) at Jicamarca station. On February 28th between 03:20 and 19:00 UT (LT = UT-5), we can observe an abnormal increase in the vertical drift compared to the values of the subsequent days (see shadowed region in Figure 8).

Based on these observations, the positive phase of the ionospheric storm at the Tucumán station is generated by the disturbance dynamo electric field (DDEF) mechanism, which enhances the upward vertical drift and leads to a super-source effect on 28th February.

In support of this interpretation, Tariq et al. (2024) analyzed the February 2023 geomagnetic storm and reported an EEJ enhancement over the American sector, accompanied by signatures of the DIS effect. Although their study was based on data from different stations, the reported EEJ enhancement occurred at a longitude very close to Jicamarca, approximately 30° to the east, which corresponds to about 2 hr in local time (as shown in their Figure 10). Therefore, their results are consistent with the physical scenario proposed in our work, reinforcing the role of DDEF-driven vertical drifts and the associated superfountain mechanism.

In the Antarctic region, the enhancement of TEC (Figure 5) is observed in parallel with the positive phase of the ionospheric storm in Tucuman on 28th February. A similar enhancement is seen for O/N_2 for the mentioned region (see Antarctic Peninsula in Figure 6), as well as in Figure 7, which shows the corresponding increase of TEC in the region at 60–70°S between 09:00 and 20:00 LT.

We suggest that some transport mechanisms are acting from low to higher latitudes. Nevertheless, further data and analysis are needed to explain better. Not only the F-region in the ionosphere is perturbed during space weather events. At D-region altitudes (75–95 km), the enhancement of electron density may cause the increase of non-derivative absorption impacting HF radio (3–30 MHz) radio wave signals. The “auroral absorption” (AA) or “auroral blackout” occurs during geomagnetic storms in the polar region (Rishbeth & Garriott, 1969).

This HF signal absorption is the result of the interactions between radio waves and the ionospheric particles where the radio waves's energy is transferred to charged particles and in turn, they can be lost because of collisions with neutral particles. Neutral particle density is higher in the D-region than in the E or F-region which increases the rate of particle collisions producing the radio waves to be absorbed and thus, the radio links are affected (Hargreaves, 1969).

The solar wind-magnetosphere-ionosphere coupling during space weather events intensifies particle precipitation leading to enhanced ionization in the ionosphere at auroral latitudes, This AA event has its peaks between 64° and

68° geomagnetic latitudes but this may vary according to the space weather conditions affecting close regions and typic. Vernadsky is at ~55.9°S and often during intense or long-lasting geomagnetic storms exhibits this type of AA event.

According to Fiori et al. (2022), statistically, AA events may last between 5 and 12 hr (mean occurrence values) during geomagnetic storms with Kp = 8 to 9. However, in our study, we observed 25 hr of AA, in this case with a Kp = 6. This regional feature explains the gap in ionosonde data observed in Figures 3 and 4 at Vernadsky station. Moreover, Figure 5 shows TEC values for the same station confirming that ionosonde radio-waves blackout is due to D-layer absorption while satellite data is able to produce measurements highlighting the need for combined multi-instrumental data analysis.

6. Conclusions

In this work, we analyzed the global and regional ionospheric perturbations observed as a response to the moderate geomagnetic storm on 26 February 2023 (Kp = 6). We analyzed space-based data for the solar-wind-magnetosphere coupling, geomagnetic indices, and ground-based data from ionosonde and ISR, and vTEC derived from GNSS for the upper atmosphere. This multi-instrumental approach aims to analyze the ionospheric response from Antarctica to the Equatorial region in South America.

We discussed the global response during the main phase of the geomagnetic storm. We observed a negative phase ionospheric storm (foF2 decreased more than 30% with respect to the reference levels) caused by PPEF and changes in the composition of the thermosphere using ionosonde data, TEC, and GUVI maps. At the Antarctic station, Vernasky, we also observed a response at the D-layer heights caused by an ionization enhancement causing high absorption of HF signals.

In addition, at the equatorial region (Tucumán), during the recovery phase of the geomagnetic storm, a significant enhancement in foF2 (>30% compared with the reference curve) is observed during the daytime. Using vTEC maps and vertical drift from ISR at Jicamarca, we showed the occurrence of an enhanced EIA effect on 28th February. The main mechanism acting in this regional effect (enhanced EIA) is attributed to DDEF.

For the determination of the effects of a geomagnetic storm from a quiet curve, we emphasize the importance of considering local ionospheric regimes both spatially and temporally, such as the WSA at Vernadsky.

In this study, we highlighted the importance of studying both the global and regional response of the ionosphere to space weather events as well as the use of a multi-instrumental approach.

Data Availability Statement

We gratefully acknowledge SWPC-NOAA (https://www.ngdc.noaa.gov/), the Kyoto World Data Center (WDC) for Geomagnetism (https://wdc.kugi.kyoto-u.ac.jp/), the GFZ German Research Centre for Geosciences (https://kp.gfz-potsdam.de/), and the Program Embrace/INPE (https://www2.inpe.br/climaespacial) for producing and providing data from solar wind parameters and geomagnetic índices. Global Navigation Satellite System (GNSS) receivers 178 data by calibrating the Receiver Independent Exchange (RINEX) format using GPS-TEC software 179 version 2.9.5 developed by Gopi Seemala (Seemala & Valladares, 2011, p. 180 http://seemala.blogspot.com). GNSS data were downloaded from the 184 International GNSS Service network (IGS, www.igs.org; Dow et al., 2009), from the Low-Latitude 185 Ionospheric Sensor Network (LISN, http://lisn.igp.gob.pe), from the Rede Brasileira de 186 Monitoramento Contínuo de Sistemas GNSS (RBMC, www.ibge.gov.br), from the Red Argentina 187 de Monitoreo Satelital Continuo (RAMSAC, www.ign.gob.ar; Piñón et al., 2018) and from Centro 188 Sismológico Nacional network (CSN, www.sismologia.cl). GUVI maps were dowloaded from https://guvitimed.jhuapl.edu/. Ionospheric parameters were provided by Radio Observatorio de Jicamarca (https://www.igp.gob.pe/observatorios/radio-observatorio-jicamarca) and electronic Space Weather upper atmosphere eSWua from INGV (http://www.eswua.ingv.it/).

Acknowledgments
This research was supported by funding from Universidad Nacional de Tucumán (Grant PIUNT E-734), Facultad Regional Bahía Blanca and Tucumán from the Universidad Tecnológica Nacional (Grant PID 10131), and from CONICET. The first author, Y. M. Melendi, would like to thank the Universidad Nacional del Sur, the Instituto de Física del Sur, and the TSWC for their support and collaboration during this research. Author M. Bravo acknowledges ANID/FONDECYT Regular 1211144. We would like to thank the SWPC-NOAA, WDC Center for Geomagnetism, GFZ-Postdam, INPE, IGS, LISN, RBMC, RAMSAC, CSN for providing the data used in this research.

References

Aa, E., Zhang, S.-R., Wang, W., Erickson, P. J., & Coster, A. J. (2023). Multiple longitude sector storm-enhanced density (SED) and long-lasting subauroral polarization stream (SAPS) during the 26–28 February 2023 geomagnetic storm. *Journal of Geophysical 16 Space Physics*, *128*(9), e2023JA031815. https://doi.org/10.1029/2023JA031815

Ambili, K. M., & Choudhary, R. K. (2023). The role of the storm-time prompt penetrating electric field on the net distribution of plasma density over the low latitude ionospheric regions. *Advances in Space Research*, *72*(5), 1644–1655. https://doi.org/10.1016/j.asr.2023.04.046

Appleton, E. V. (1946). Two anomalies in the ionosphere. *Nature*, *157*(3995), 691. https://doi.org/10.1038/157691a0
Balan, N., Shiokawa, K., Otsuka, L., Kukuchi, T., Lekshmi, D. V., Kawamura, S., et al. (2010). A physical mechanism of positive ionospheric storms at low latitudes and midlatitudes. *Journal of Geophysical Research*, *115*(A2), A02304. https://doi.org/10.1029/2009JA014515
Bellchambers, W. H., & Piggott, W. R. (1958). Ionospheric measurements made at Halley Bay. *Nature*, *182*(4649), 1596–1597. https://doi.org/10.1038/1821596a0
Bianchi, C., Baskaradas, J., Pezzopane, M., Pietrella, M., Umberto, S., & Zuccheretti, E. (2013). Fading in the HF ionospheric channel and the role of irregularities. *Advances in Space Research*, *52*(3), 403–411. https://doi.org/10.1016/j.asr.2013.03.035
Bojilova, R., & Mukhtarov, P. (2023). Analysis of the ionospheric response to sudden stratospheric warming and geomagnetic forcing over Europe during February and March 2023. *Universe*, *9*(8), 351. https://doi.org/10.3390/universe9080351
Bravo, M. A., Villalobos, C. U., Castillo-Rivera, C. A., Foppiano, A. J., & Ovalle, E. M. (2025). Seasonal evolution of the ionospheric summer evening and Weddell Sea Anomalies: Antarctic Peninsula area. *Advances in Space Research*, *75*(6), 4740–4755. https://doi.org/10.1016/j.asr.2024.12.047
Buonsanto, M. J. (1999). Ionospheric storms– A review. *Space Science Reviews*, *88*(3/4), 563–601. https://doi.org/10.1023/A:1005107532631
Cabrera, M., Zuccheretti, E., Ezquer, R., Sciacca, U., Lopez, J., Molina, M., & Baskaradas, J. (2010). Some considerations for different time-domain signal processing of pulse compression radar. *Annals of Geophysics*, *53*(5–6), 1–11. https://doi.org/10.4401/ag-4758
Cander, L. R., & Mihajlovic, S. J. (1998). Forecasting ionospheric structure during the great geomagnetic storms. *Journal of Geophysical Research*, *103*(A1), 391–398. https://doi.org/10.1029/97JA02418
Chang, L. C., Liu, H., Miyoshi, Y., Chen, C.-H., Chang, F.-Y., Lin, C.-H., et al. (2015). Structure and origins of the Weddell SeaAnomaly from tidal and planetary wave signatures in FORMOSAT-3/COSMIC observations and GAIAGCM simulations. *Journal of Geophysical Research: Space Physics*, *120*(2), 1325–1340. https://doi.org/10.1002/2014JA020752
Danilov, A. D. (2001). F2-region response to geomagnetic disturbances. *Journal of Atmospheric and Solar-Terrestrial Physics*, *63*(5), 441–449. https://doi.org/10.1016/S1364-6826(00)00175-9
Danilov, A. D. (2013). Ionospheric F-region response to geomagnetic disturbances. *Advances in Space Research*, *52*(3), 343–366. https://doi.org/10.1016/j.asr.2013.04.019
Danilov, A. D., & Lastovicka, J. (2001). Effects of geomagnetic storms on the ionosphere and atmosphere. *International Journal of Geomagnetism and Aeronomy*, *3*(2), 201–224.
Denardini, C. M., Da Silva, M. R., Gende, M., Su Chen, S., Fagundes, P. R., Schuch, N. J., et al. (2015). The initial steps for developing the South American K index from the embrace magnetometer network. *Revista Brasileira de Geofísica*, *33*(1), 79–88. https://doi.org/10.1590/rbgf.v33i1.603
Dow, J. M., Neilan, R. E., & Rizos, C. (2009). The international GNSS service in a changing landscape of global navigation satellite systems. *Journal of Geodesy*, *83*(3–4), 191–198. https://doi.org/10.1007/s00190-008-0300-3
Fang, H., Weng, L., & Sheng, Z. (2012). Variations in the thermosphere and ionosphere response to the 17–20 April 2002 geomagnetic storms. *Advances in Space Research*, *49*(10), 1529–1536. https://doi.org/10.1016/j.asr.2012.02.024.17
Fiori, R. A. D., Kumar, V. V., Boteler, D. H., & Terkildsen, M. B. (2022). Occurrence rate and duration of space weather impacts on high-frequency radio communication used by aviation. *Journal of Space Weather and Space Climate*, *12*, 21. https://doi.org/10.1051/swsc/2022017
Gonzalez, W., Joselyn, J.-A., Kamide, Y., Kroehl, H. W., Rostoker, G., Tsurutani, B., & Vasyliunas, V. (1994). What is a geomagnetic storm? *Journal of Geophysical Research*, *99*(A4), 5771–5792. https://doi.org/10.1029/93JA02867
Hargreaves, J. K. (1969). Auroral absorption of HF radio waves in the ionosphere: A review of results from the first decade of riometry, In *Proceedings of the IEEE*, Vol. 57(8) pp. 1348–1373. https://doi.org/10.1109/PROC.1969.7275
Huang, H., Lu, X., Liu, L., Wang, W., & Li, Q. (2018). Transition of interhemispheric asymmetry of equatorial ionization anomaly during solstices. *Journal of Geophysical Research: Space Physics*, *123*(12), 10283–10300. https://doi.org/10.1029/2018JA026055
Ippolito, A., Perrone, L., Plainaki, C., & Cesaroni, C. (2020). Investigating the foF2 variations at the ionospheric observatory of rome during different solar cycles minimums and levels of geomagnetic activity. *Journal of Space Weather and Space Climate*, *10*, 52. https://doi.org/10.1051/swsc/2020054
Kane, R. P. (2005). Ionospheric foF2 anomalies during some intense geomagnetic storms. *Annals of Geophysics*, *23*(7), 2487–2499. https://doi.org/10.5194/angeo-23-2487-2005
Karpachev, A. T., Gasilov, N. A., & Karpachev, O. A. (2011). Morphology and causes of the Weddell anomaly. *Geomagnetism and Aeronomy*, *51*(6), 812–824. https://doi.org/10.1134/S0016793211050070
Koloskov, O., Kashcheyev, A., Bogomaz, O., Sopin, A., Gavrylyuk, B., & Zalizovski, A. (2023). Performance analysis of a portable low-cost SDR-based ionosonde. *Atmosphere*, *14*(1), 159. https://doi.org/10.3390/atmos14010159
Kutiev, I., & Muhtarov, P. (2001). Modeling of midlatitude F-region response to geomagnetic activity. *Journal of Geophysical Research*, *106*(A8), 15501–15509. https://doi.org/10.1029/2001JA900018
Mikhailov, A. V., & Perrone, L. (2009). Pre-storm NmF2 enhancements at middle latitudes: Or reality. Annals of Geophysics, *27*(3), 1321–1330. https://doi.org/10.5194/angeo-27-1321-2009
Mikhailov, A. V., Skoblin, M. G., & Forster, M. (1995). Daytime F2-layer positive storm effect at middle and lower latitudes. *Annals of Geophysics*, *13*(5), 532–540. https://doi.org/10.1007/s00585-995-0532-y
Molina, M. G., Dasso, S., Mansilla, G., Namour, J. H., Cabrera, M. A., & Zuccheretti, E. (2020). Consequences of a solar wind stream interaction region on the low latitude ionosphere: Event of 7 October 2015. *Solar Physics*, *295*(12), 173. https://doi.org/10.1007/s11207-020-01728-7
Molina, M. G., Zuccheretti, E., Cabrera, M. A., Bianchi, C., Sciacca, U., & Baskaradas, J. (2016). Automatic ionospheric layers detection: Algorithms analysis. *Advances in Space Research*, *57*(6), 1360–1372. https://doi.org/10.1016/j.asr.2015.10.022
Mošna, Z., Barta, V., Berényi, K. A., Mielich, J., Verhulst, T., Kouba, D., et al. (2024). The March and April 2023 ionospheric storms over Europe. *Frontiers in Astronomy and Space Sciences*, *11*, 1462160. https://doi.org/10.3389/fspas.2024.1462160
Nayak, C., Tsai, L.-C., Su, S.-Y., Galkin, I. A., Tan, A. T. K., Nofri, E., & Jamjareegulgarn, P. (2016). Peculiar features of the low-latitude and midlatitude ionospheric response to the st. Patrick's Day geomagnetic storm of 17 March 2015. *Journal of Geophysical Research: Space Physics*, *121*(8), 7941–7960. https://doi.org/10.1002/2016JA022489
Piñón, D. A., Gómez, D. D., Smalley, R., Cimbaro, S. R., Lauría, E. A., & Bevis, M. G. (2018). The history, State, and future of the Argentine continuous satellite monitoring network and its contributions to geodesy in Latin America. *Seismological Research Letters*, *89*(2A), 475–482. https://doi.org/10.1785/0220170162
Prölss, G. W. (1995). Ionospheric F-region storms. In H. Volland (Ed.), *Handbook of atmospheric electrodynamics* (Vol. 2, pp. 195–248). CRC Press.

Reznychenko, M., Kotov, D., Bogomaz, O., Zhivolup, T., Reznychenko, A., Zalizovski, A., et al. (2024). Ionospheric response to the February 27, 2023 intense geomagnetic storm over Kharkiv and the Akademik 18 station. *Ukrainian Antarctic Journal*, *22*(1), 40–50. https://doi.org/10.33275/1727-7485.1.2024.726

Richmond, A. D. (2021). Joule heating in the thermosphere. *Geophysical Monograph Series*, 1–18. https://doi.org/10.1002/9781119815631.ch1

Rishbeth, H. (1991). F-region storms and thermospheric dynamics. *Journal of Geomagnetism and Geoelectricity*, *43*(Supplement1), 513–524. https://doi.org/10.5636/jgg.43.supplement1_513

Rishbeth, H., & Garriott, O. K. (1969). *Introduction to ionospheric physics. Amsterdam*. Academic Press.

Rishbeth, H., Heelis, R. A., Makela, J. J., & Basu, S. (2010). Storming the bastille: The effect of electric fields on the ionospheric F-layer. *Annals of Geophysics*, *28*(4), 977–981. https://doi.org/10.5194/angeo-28-977-2010

Scherliess, L., & Fejer, B. G. (1997). Storm time dependence of equatorial disturbance dynamo zonal electric fields. *Journal of Geophysical Research*, *102*(A12), 24037–24046. https://doi.org/10.1029/97ja02165

Scotto, C., & Pezzopane, M. (2000). A software for automatic scaling of foF2 and MUF(3000)F2 from ionograms. *Proc. URSI*, 217–242.

Seemala, G. K., & Valladares, C. E. (2011). Statistics of total electron content depletions observed over the South American continent for the year 2008. *Radio Science*, *46*(5), RS5019. https://doi.org/10.1029/2011RS004722

Starodubtsev, S. A., Gololobov, P. Y., Grigoryev, V. G., & Zverev, A. S. (2024). MHD waves in solar wind plasma during geomagnetic storm events in February–March 2023 (2024). *Cosmic Research*, *62*(2), 178–186. https://doi.org/10.1134/S0010952523600312

Sun, W., Li, G., Lei, J., Zhao, B., Hu, L., Zhao, X., et al. (2023). Ionospheric super bubbles near sunset and sunrise during the 26–28 February 2023 geomagnetic storm. *Journal of Geophysical Research: Space Physics*, *128*(11), e2023JA031864. https://doi.org/10.1029/2023JA031864

Tanaka, T., & Ohtaka, K. (1996). Ionospheric disturbances during low-latitude auroral events and their association with magnetospheric processes. *Journal of Geophysical Research*, *101*(A8), 17151–17159. https://doi.org/10.1029/96JA00832

Tariq, M. A., Liu, L., Shah, M., Yang, Y., Sun, W., Ali Shah, M., et al. (2024). Longitudinal variations of ionospheric responses to the February and April 2023 geomagnetic storms over American and Asian sectors. *Advances in Space Research*, *73*(6), 3033–3049. https://doi.org/10.1016/j.asr.2023.12.039

Tsagouri, I., Belehaki, A., Moraitis, G., & Mavromichalaki, H. (2000). Positive and negative ionospheric disturbances at middle latitudes during geomagnetic storms. *Geophysical Research Letters*, *21*, 3579–3582. https://doi.org/10.1029/2000GL003743

Tsurutani, B. T., Lakhina, G. S., & Hajra, R. (2020). The physics of space weather/solar-terrestrial physics (STP): What we know now and what the current and future challenges are. *Nonlinear Processes in Geophysics*, *27*(1), 75–119. https://doi.org/10.5194/npg-27-75-2020

Tsurutani, B. T., Verkhoglyadova, O. P., Mannucci, A. J., Saito, A., Araki, T., Yumoto, K., et al. (2008). Prompt penetration electric fields (PPEFs) and their ionospheric effects during the great magnetic storm of 30–31 October 2003. *Journal of Geophysical Research*, *113*(A5), A05311. https://doi.org/10.1029/2007JA012879

Wang, W., Burns, A. G., & Liu, J. (2021). Upper thermospheric winds: Forcing, variability, and effects. In *In upper atmosphere dynamics and energetics* (pp. 41–63). https://doi.org/10.1002/9781119815631.ch3

Werner, S., Bauske, R., & Prolss, G. W. (1999). On the origin of positive ionospheric storms. *Advances in Space Research*, *24*(11), 1485–1489. https://doi.org/10.1016/S0273-1177(99)00711-5

Yang, N., Yu, T., Le, H., Liu, L., Sun, Y.-Y., Yan, X., et al. (2022). The feature of ionospheric mid-latitude trough during geomagnetic storms derived from GPS total electron content (TEC) data. *Remote Sensing*, *14*(2), 369. https://doi.org/10.3390/rs14020369

Zalizovski, A., Stanislawska, I., Lisachenko, V., & Charkina, O. (2021). Variability of Weddell Sea ionospheric anomaly as deduced from observations at the Akademik Vernadsky station. *Ukrainian Antarctic Journal*(1), 47–55. https://doi.org/10.33275/1727-7485.1.2021.666

Zolesi, B., & Cander, J. (2014). *Ionospheric prediction and forecasting*. Springer. https://doi.org/10.1007/978-3-642-38430-1